mathematics

MDPI

Article

Bilevel Optimal Sizing and Operation Method of Fuel Cell/Battery Hybrid All-Electric Shipboard Microgrid

Hao Jin * and Xinhang Yang

School of Engineering, University of Glasgow, Glasgow G12 8QQ, UK; 2758147y@student.gla.ac.uk
* Correspondence: 2726225J@student.gla.ac.uk

Abstract: The combination of transportation electrification and clean energy in the shipping industry has been a hot topic, and related applications of hybrid all-electric ships (AESs) have emerged recently. However, it has been found that ship efficiency will be negatively impacted by improper component size and operation strategy. Therefore, the bilevel optimal sizing and operation method for the fuel cell/battery hybrid AES is proposed in this paper. This method optimizes the sizing of the AES while considering joint optimal energy management and voyage scheduling. The sizing problem is formulated at the upper level, and the joint scheduling problem is described at the lower level. Then, multiple cases are simulated to verify the effectiveness of the proposed method on a passenger ferry, and the results show that a 5.3% fuel saving and 5.2% total cost reduction can be achieved. Correspondingly, the ship's energy efficiency is improved. This approach also can be used in similar vessels to enhance their overall performance and sustainability.

Keywords: sizing; fuel cell/battery hybrid ship; zero-emission; all-electric ship (AES); energy management; voyage scheduling

MSC: 90c90

Citation: Jin, H.; Yang, X. Bilevel Optimal Sizing and Operation Method of Fuel Cell/Battery Hybrid All-Electric Shipboard Microgrid. *Mathematics* **2023**, *11*, 2728. https://doi.org/10.3390/math11122728

Academic Editors: Rui Wang and Shi Cheng

Received: 20 May 2023
Revised: 14 June 2023
Accepted: 15 June 2023
Published: 16 June 2023

1. Introduction

Over the past ten years, the problem of reducing emissions has been critical in the shipping industry. Although more than 80% of global trade was undertaken by international shipping, about 3% of global greenhouse gas (GHG) emissions were emitted by the shipping industry [1]. To tackle this issue, in 2018, the International Maritime Organization (IMO) proposed an ambitious target to reduce the annual GHG emissions for global shipping by at least 50% by 2050 compared to 2008 [2,3]. In order to meet this goal, various new technologies have been proposed and investigated on board [4–6]. Among them, the all-electric ship (AES), which has superior efficiency and flexibility by distributing the electricity power uniformly, is considered one of the most promising technologies, and has been extensively studied [7–11]. In this paper, the zero-emission AES utilizing clean and renewable energy sources will be investigated.

With the advancements in fuel cell technology and hydrogen production and storage, there has been a rise in the number of hydrogen-fuel-cell-powered ships [12–15]. For small ferry boats, zero-emission AESs with hydrogen fuel cells (FCs) and battery integration are receiving more attention [16]. One of the key benefits of using FCs is that there is no direct GHG emission during usage, making it a much cleaner alternative to diesel generators (DGs) [2]. In addition, its noise and vibrations are much lower, and the efficiency of electricity generation is much higher. However, considering the FC's characteristics of low dynamic reaction, batteries are usually integrated on board to cover the sudden load variation, which also can be used to achieve the balance between power sources and loads to improve the system's flexibility further [17,18].

Contrary to the research on the optimal operation of land-based microgrids, which only considers energy management [19], it is common for scholars to focus on optimizing

both energy management and voyage scheduling in the field of all-electric shipboard microgrids to improve the overall energy efficiency [11,20–23]. Since energy management and voyage scheduling in the AESs are coupled due to the relationship between propulsion loads and ship speed, Shang et al. [20] formulated a multi-objective optimization model to achieve the joint generation and voyage scheduling for an AES with the integration of diesel generators and energy storage systems (ESSs). The results show that joint scheduling could reduce operational costs and GHG emissions simultaneously compared to fixed voyage scheduling. Huang et al. [21] regarded thermal storage and load as a virtual ESS, and proposed a multi-objective optimization model to optimize the voyage scheduling and power generation of the AES coordinately. The results also show the superiority of the joint optimization method over the fixed voyage scheduling methods.

ESS sizing based on the joint optimal generation–voyage scheduling has also been investigated in some studies [24–26]. Considering that a single ESS deployment ship may not meet the increasingly stringent regulation of GHG emissions in the future, Fang et al. [24] chose to install the carbon capture system (CCS) and ESS on board, and introduced a two-stage planning method to determine the optimal capacity. The capacity of CCS and ESS is determined in the first stage. Then, the joint scheduling is implemented in the second stage under the given capacity of components. Wen et al. [25] presented a biobjective bilevel optimization method to optimize voyage routing and ESS sizing coordinately based on solar power prediction. Zhao et al. [26] proposed a biobjective optimization model to optimize ESS size and voyage routine, considering the uncertainty of onshore electricity prices. However, the research objectives in these studies are the diesel/battery hybrid ship, which differs from the fuel cell/battery hybrid ship.

In the previous studies of fuel cell/battery hybrid AESs, some scholars focused on the energy management of the shipboard microgrid [17,27–30]. Banaei et al. [17] proposed an optimal energy management strategy considering different operation constraints of FCs and batteries. Then, the model predictive control (MPC) method was used to reduce the load forecast error. Some studies focus on the sizing of FC and battery on board [18,31]. Letafat et al. [18] investigated the energy management and component sizing method for the fuel cell/battery hybrid AES to minimize the total cost, including the operation cost and daily investment cost. The result shows that the sizes of FCs and batteries can be determined effectively while optimal energy management is achieved. Wang et al. [31] proposed a method to optimize the sizing of diesel engines, batteries, fuel cells, and energy management of a hybrid offshore support vessel. However, only energy management is considered in these sizing methods, and the voyage and load profiles are predetermined. Motivated by this problem, Pan et al. [32] proposed a hybrid energy configuration method based on the coordinated navigation routing and power generation scheduling model to optimize the capacity of the battery and FC. Nevertheless, the research objective of the passenger ferry in this paper usually has a fixed time window different from the cargo ship studied in [32].

The purpose of this paper is to propose an optimization method to determine the optimal component size for a fuel cell/battery hybrid ferry while optimizing the generation–voyage scheduling. This method can be used to offer guidance to the designer during the early stages of the ship design and building process, as well as to provide information to ship owners before the voyage. Our main contributions are twofold: (1) an optimal sizing and operation framework is proposed based on the bilevel optimization model; (2) a bilevel optimal sizing and operation method for the fuel cell/battery hybrid AES is proposed. At the upper level, the sizes of the components are optimized to minimize the total cost, while the energy management and voyage scheduling are optimized jointly at the lower level to minimize the operation cost, considering the constraints related to the practical operation of AESs, i.e., the output constraint, the ramp rate constraint, and the spinning reserve constraint.

The rest of this article is organized as follows. In Section 2, the problem is stated, and the framework of the proposed method is described. In Section 3, the mathematical

model of AES and hydrogen fuel cell is established. In Section 4, the problem is formulated, and the solution algorithm is described. In Section 5, the solution algorithm is detailed. In Section 6, the numerical experiments are investigated, and their results are analyzed. Finally, conclusions are presented in Section 7.

2. Problem Statement

2.1. Topology of the AES

The topology of the shipboard microgrid of the AES is illustrated in Figure 1. The power of the fuel cell and the battery is distributed by the power network to satisfy the demand of propulsion and service loads on board. The fuel cell supplied by the hydrogen tank is selected as the primary energy source. The battery is used to balance the power source and loads, which ensures that the FCs can be operated at their optimal operating point and improves the flexibility of the ship's operation. Specifically, when the output power of the FCs exceeds the load demand, the battery will be charged. Conversely, when the load demand exceeds the output power of the FCs, the battery will be discharged. In addition, when the ship anchors at the port, the cold ironing can be connected to the shipboard microgrid to supply electricity to service loads and charge the battery. The loads on board involve the propulsion loads of two waterjet engines and service loads of lighting, radar, and air conditioning.

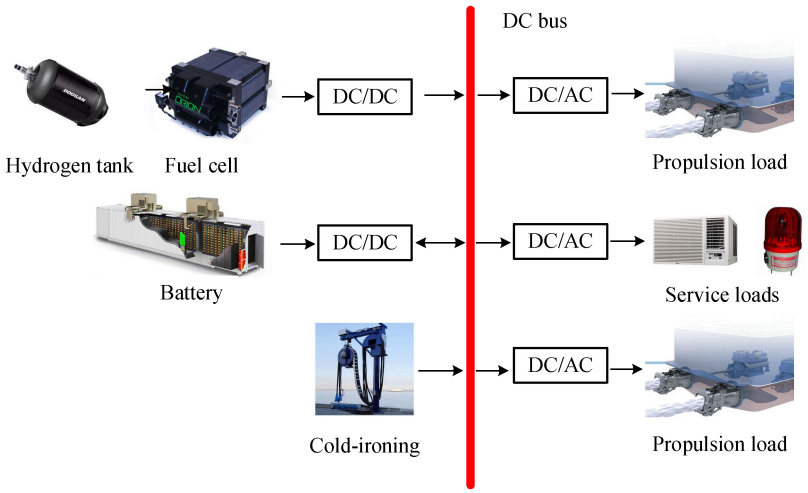

Figure 1. Topology of fuel cell/battery AES.

2.2. Framework of Proposed Method

The framework of the proposed method is given in Figure 2. The optimization of the design and operation for a fuel cell/battery hybrid ferry are closely connected. However, combining these problems into a single optimization challenge can result in an overwhelming number of variables and constraints that are difficult to solve computationally [33]. The bilevel optimization model has been proposed by researchers to solve similar problems, and is reported to exhibit good performance [24,25,32]. It is adopted in this paper to solve the problem of excessive variables and constraints. Bilevel optimization models are characterized by two optimization problems that are hierarchically related [34]. In such problems, an optimal solution in the lower-level problem must be associated with each feasible upper-level solution. In this paper, the upper level is used to determine the optimal sizing of the FC and battery while minimizing the total cost, which includes the investment cost of the FC and battery and operation cost at the lower level. The optimal operation of the AES is investigated at the lower level. With the given capacity of components from the upper level, the lower level is used to minimize the operation cost by determining the optimal ship speed and hourly output power of the FC and battery. Then, the joint optimization of energy management and voyage scheduling is achieved for the AES. Finally, the optimal results are sent to the upper level to determine the optimal sizes of the components. In

addition, the optimization problems of the upper and lower level are solved by the particle swarm optimization (PSO) algorithm and mixed-integer linear programming (MILP) solver.

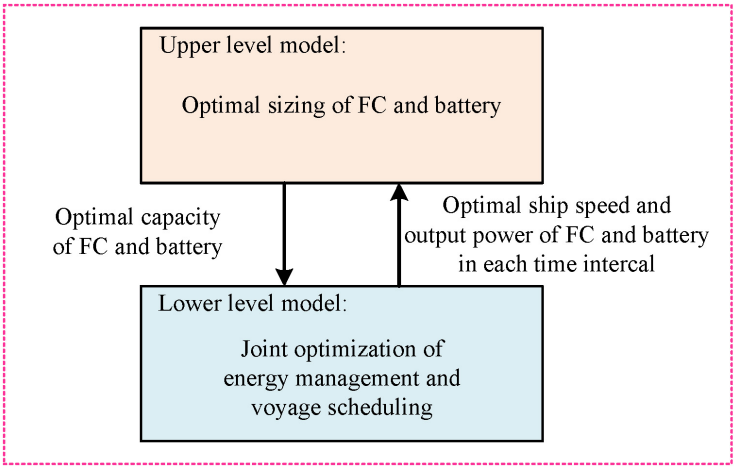

Figure 2. Framework of proposed optimal sizing method based on bilevel optimization model.

3. Mathematical Modeling

3.1. AES Voyage Model

In order to investigate the optimal voyage scheduling, the AES voyage model is established, which follows a specific voyage pattern, as illustrated in Figure 3. The ship departs from port 1 to visit intermediate ports 2 and 3 and returns to port 1. The voyage for the AES lasts for T time intervals, and the duration of each interval is Δt. The state of the ship during the voyage can be divided into three types based on the ship speed: the ship cruises at full speed in the period T_c; the ship cruises with a lower speed in the period T_p; the ship berths at the port in the period T_b. The periods T_c, T_p, and T_b are denoted as full-speed cruising, partial-speed cruising, and berthing periods, respectively. It is noted that there are three different ship speed constraints according to the three different periods. The voyage distance at the t-th time interval can be updated using Equation (1). The propulsion load is calculated according to the exponential relationship between propulsion load and cruising speed, as shown in Equation (2) [20,35].

$$Dist_t = \begin{cases} Dist_{t-1} + v_t \Delta t & t \in T \backslash \{1\} \\ v_t \Delta t & t = 1 \end{cases} \tag{1}$$

$$P_t^{pl} = c_1 \cdot (v_t)^{c_2} \tag{2}$$

where $Dist_t$ is the voyage distance at the t-th time interval; v_t is the ship cruising speed in the t-th time interval; Δt is the voyage time at the t-th time interval; P_t^{pl} is the power demand of propulsion load; c_1 and c_2 are the proportional and exponential coefficients of the propulsion–speed relationship, respectively; t is the t-th time interval; T is the number of time intervals.

3.2. Hydrogen Fuel Cell Operation Model

In this section, the relationship between the output power of the FC and the consumed mass of hydrogen is analyzed. During the voyage, the hydrogen stored in the tank will be consumed by the FC to output electric power. In this paper, a coefficient is used to convert the mass of hydrogen into the FC's generated power. Moreover, the FC's generated power is not equal to the FC's output power, as there is conversion efficiency between them. The efficiency curve is illustrated in Figure 4, where the efficiency of the FC changes with the variation in its output power. As a result, a nonlinear relationship exists between the FC's generated and output power.

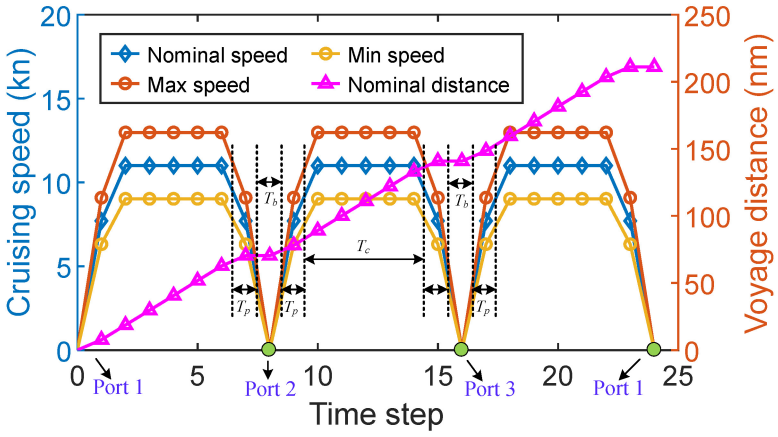

Figure 3. Voyage pattern of an all-electric ship (AES).

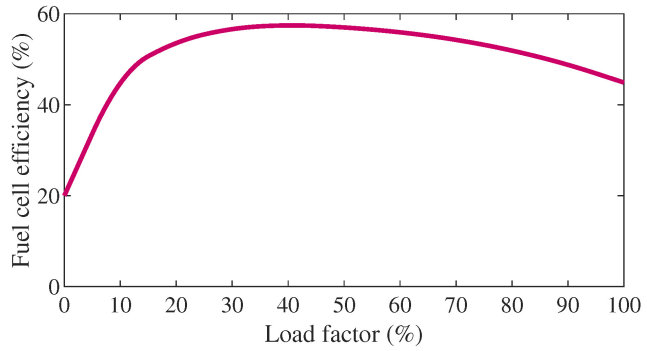

Figure 4. Efficiency curve of FC.

In this paper, a linear fitting function is employed to describe this relationship, as shown in Equation (3) [27]. Ultimately, with the given output power of the FC, the consumed mass of hydrogen can be calculated.

$$M_t^{H_2} = K^{E-m} P_t^{FC,gen} = K^{E-m}\left(\alpha^{FC} P_t^{FC} + o_t^{FC}\beta^{FC}\right), \forall t \in T \tag{3}$$

where $M_t^{H_2}$ is the consumed mass of hydrogen at the t-th time interval; $P_t^{FC,gen}$ and P_t^{FC} are the generated power and output power of fuel cell, respectively; K^{E-m} is the coefficient used to convert the generated power of the fuel cell into the mass of hydrogen; α^{FC} and β^{FC} are the fitting coefficients of the relationship between $P_t^{FC,gen}$ and P_t^{FC}; o_t^{FC} is the on/off state at the t-th time interval, $o_t^{FC} \in \{0,1\}, \forall t \in T$.

4. Problem Formulation

4.1. Upper Level

In this section, the bilevel optimal sizing and operation model is established for the fuel cell/battery hybrid AES.

4.1.1. Objective Function

The objective of the upper level is to minimize the total cost of the fuel cell/battery hybrid AES by determining the optimal sizing of the FC and battery, which is given as follows:

$$\min C = C_{INV} + C_{OP} \tag{4}$$

where C is the total cost of a single voyage, which includes the investment cost C_{INV} and operation cost C_{OP}. In this paper, the investments of the FC and battery are unified into a single voyage, which can be calculated by Equations (5) and (11), respectively.

$$C_{INV} = C_{INV}^{FC} + C_{INV}^{bat} = \frac{P_{\max}^{FC} \lambda_{INV}^{FC} T_{op}^{FC}}{T_{op,lifetime}^{FC}} + \frac{\left(\lambda_{INV}^{bat,E} E_{\max}^{bat} + \lambda_{INV}^{bat,P} P_{\max}^{bat}\right) N^{bat,cycle}}{N_{lifetime}^{bat,cycle}} \quad (5)$$

where C_{INV}^{FC} and C_{INV}^{bat} are the total investment cost of the fuel cell and battery, respectively; λ_{INV}^{FC}, $\lambda_{INV}^{bat,E}$, and $\lambda_{INV}^{bat,P}$ are the price of the fuel cell power (\$/kW), battery capacity (\$/kWh), and battery power (\$/kW), respectively; T_{op}^{FC} and $T_{op,lifetime}^{FC}$ are the operation times of the fuel cell for a single voyage and its lifetime, respectively; $N^{bat,cycle}$ and $N_{lifetime}^{bat,cycle}$ are the battery charging/discharging cycle numbers for a single voyage and its lifetime, respectively. T_{op}^{FC} and $N^{bat,cycle}$ can be calculated using Equations (6) and (7).

$$T_{op}^{FC} = \sum_{t \in T} o_t^{FC} \quad (6)$$

$$N^{bat,cycle} = \min\left(\sum_{t \in T}\left(X_t^{ch}\right), \sum_{t \in T}\left(1 - X_t^{ch}\right)\right) \quad (7)$$

where X_t^{ch} is battery charging/discharging state at the t-th time interval, $X_t^{ch} \in \{0, 1\}, \forall t \in T$.

4.1.2. Constraints

The constraints in the upper level are mainly related to the capacity, which is determined by the limited onboard space, as shown in Equations (8)–(10).

$$0 \le P_{\max}^{bat} \le P_{sizing}^{bat} \quad (8)$$

$$0 \le E_{\max}^{bat} \le E_{sizing}^{bat} \quad (9)$$

$$0 \le P_{\max}^{FC} \le P_{sizing}^{FC} \quad (10)$$

where $P_{\max}^{bat}$ and $E_{\max}^{bat}$ are the maximum power and capacity of the battery, respectively; $P_{\max}^{FC}$ is the maximum power of the fuel cell; P_{sizing}^{bat} and E_{sizing}^{bat} are the maximum sizing power and capacity of the battery, respectively; P_{sizing}^{FC} is the maximum sizing power of the fuel cell.

4.2. Lower Level

4.2.1. Objective Function

The objective function of the lower level is to minimize the operation cost, C_{OP}:

$$\min C_{OP} = C_{H_2} + C_{CI} = \sum_{t \in T}\left(\lambda^{H_2} M_t^{H_2} + \lambda_t^{CI} P_t^{CI}\right) \quad (11)$$

where C_{H_2} and C_{CI} are the operation costs of hydrogen and cold ironing, respectively; λ^{H_2} is the hydrogen price (\$/kg); λ_t^{CI} is the cold ironing price at the t-th time interval (\$/kWh); $M_t^{H_2}$ is consumed mass of hydrogen at the t-th time interval (kg); P_t^{CI} is the output power of cold ironing at the t-th time interval.

4.2.2. Constraints

1. Power Balance Constraint

In the AES, the output powers of the FC, battery, and cold ironing need to meet the demand of the propulsion and service loads at any time interval, as shown in Equation (12)

$$\eta_T\left(P_t^{FC}+P_t^{bat,dc}+P_t^{CI}\right)=P_t^{ser}+P_t^{pl}+P_t^{bat,ch},\forall t\in T \tag{12}$$

where η_T is the transmission efficiency of shipboard microgrid; P_t^{FC} is the fuel cell output power at the t-th time interval; $P^{bat,ch}$ and $P_t^{bat,dc}$ are the battery charging power and discharging power, respectively, at the t-th time interval; P_t^{pl} and P_t^{ser} are the power demands of propulsion load and service load at the t-th time interval, respectively.

2. Fuel Cell Output Power Constraint

The output power of the FC is determined by the on/off states and the loading factor

$$P_t^{FC}=o_t^{FC}l_t^{FC}P_{\max}^{FC},\forall t\in T \tag{13}$$

where l_t^{FC} is the loading factor of the FC at the t-th time interval. In order to avoid the overloading of the FC and to prolong its life, the loading factor is limited using Equation (14).

$$l_{\min}^{FC}\le l_t^{FC}\le l_{\max}^{FC},\forall t\in T \tag{14}$$

where $l_{\min}^{FC}$ and $l_{\max}^{FC}$ are the minimum and maximum loading factors of the FC, respectively.

3. Fuel Cell Ramp Rate Constraint

Considering the characteristics of the low dynamic reaction of the FC, the variation in the FCs' output power is limited, as illustrated by Equation (15).

$$r_{\min}^{FC}P_{\max}^{FC}\le P_t^{FC}-P_{t-1}^{FC}\le r_{\max}^{FC}P_{\max}^{FC},\forall t\in T \tag{15}$$

where $r_{\min}^{FC}$ and $r_{\max}^{FC}$ are the minimum and maximum ramp rates of the FC, respectively.

4. H_2 Tank Capacity Constraint

The hydrogen tank will be fully charged in the departure port and will not be charged during the voyage. The total mass of the hydrogen consumed during the voyage cannot surpass the maximum allowable mass of the hydrogen tank, as shown in Equation (16).

$$0\le\sum_{t\in T}M_t^{H_2}\le(1-\eta_{tank})M_{\max}^{H_2} \tag{16}$$

where $M_{\max}^{H_2}$ is the maximum hydrogen tank capacity; η_{tank} is the hydrogen tank mass reserve coefficient.

5. Battery Charging and Discharging Power Constraint

The charging and discharging powers of the battery are limited to its corresponding lower and upper bound

$$0\le P_t^{bat,ch}\le X_t^{ch}P_{t,\max}^{bat},\forall t\in T \tag{17}$$

$$0\le P_t^{bat,dc}\le\left(1-X_t^{ch}\right)P_{t,\max}^{bat},\forall t\in T \tag{18}$$

6. Battery Capacity Constraint

The battery capacity at any time intervals is obtained by calculating Equations (19) and (20)

$$E_t^{bat}=E_{t-1}^{bat}+\eta_{ch}P_t^{bat,ch}-\frac{P_t^{bat,dc}}{\eta_{dc}},\forall t\backslash\{1\} \tag{19}$$

$$E_t^{bat}=E^{bat}\cdot SOC_0+\eta_{ch}P_t^{bat,ch}-\frac{P_t^{bat,dc}}{\eta_{dc}},t=1 \tag{20}$$

where E_t^{bat} is the stored energy of the battery at the t-th time interval; η_{ch} and η_{dc} are the battery charging and discharging efficiencies of the battery at the t-th time interval, respectively; SOC_0 is the initial state of charge (SOC) of the battery before the voyage, $SOC_0 = 0.5$.

7. SOC Constraint

Equation (21) is used to limit the SOC of the battery within a reasonable range.

$$(SOC_{\max} - DoD_{\max}) \le SOC_t = \frac{E_t^{bat}}{E_{\max}^{bat}} \le SOC_{\max}, \forall t \in T \tag{21}$$

where $SOC_{\max}$ is the maximum allowable SOC; $DoD_{\max}$ is the maximum allowable depth of discharge (DoD).

At the end of the voyage, the capacity of the battery should be no less than its initial capacity:

$$SOC_0 \le SOC_t \le \left(1 + \delta^{SOC}\right) SOC_0, t = T \tag{22}$$

where δ^{SOC} is the maximum allowable SOC mismatch.

8. System Reserve Constraint

In order to cope with the sudden changes in the load or outage of the FC, the reserve constraint is considered in this paper, as described in Equations (23)–(25).

$$R_t^{FC} = P_{\max}^{FC} - P_t^{FC}, \forall t \in T \tag{23}$$

$$R_t^{bat} = X_t^{ch} P_{\max}^{bat} + \left(1 - X_t^{ch}\right)\left(P_{\max}^{bat} - P_t^{bat}\right), \forall t \in T \tag{24}$$

$$R_t^{FC} + R_t^{bat} \ge \eta_R P_t^{FC}, \forall t \in T \tag{25}$$

where R_t^{FC} and R_t^{bat} are the power reserves of the FC and battery at the t-th time interval, respectively; η_R is the power reserve coefficient.

9. Cold Ironing Power Constraint

The cold ironing can be used to meet the power demand of the loads on board and to charge the battery when the ship arrives at the port, as shown in Equation (26).

$$\begin{cases} 0 \le P_t^{CI} \le P_{\max}^{CI}, & t \in T_b \\ P_t^{CI} = 0, & otherwise \end{cases} \tag{26}$$

where $P_{\max}^{CI}$ is the maximum power of cold ironing.

10. AES sailing Speed Constraint

The AES sailing speed constraints during the full-speed period T_c, the partial-speed period T_p, and the berthing period T_b are given in Equation (27).

$$\begin{cases} (1 - \delta_{\max}^v) \cdot v^n \le v_t \le (1 + \delta_{\max}^v) \cdot v^n, & \forall t \in T_c \\ \eta_p (1 - \delta_{\max}^v) \cdot v^n \le v_t \le \eta_p (1 + \delta_{\max}^v) \cdot v^n, & \forall t \in T_p \\ v_t = 0, & \forall t \in T_b \end{cases} \tag{27}$$

where v^n is the nominal sailing speed; η_p is the partial ratio; $\delta_{\max}^v$ is the maximum allowable sailing speed mismatch.

11. Voyage Constraint

The ferry investigated in this paper should arrive at each port punctually. Of course, a small quantity of mismatch with time is allowed. Thus, when the ship arrives at the

intermediate and terminal port, the voyage constraints in Equations (28) and (29) should be satisfied:

$$\left(1-\delta_{\max}^{D}\right)Dist_t^n \le Dist_t \le \left(1+\delta_{\max}^{D}\right)Dist_t^n, \forall t \in T_b \backslash \{T\} \tag{28}$$

$$Dist_T^n \le Dist_T \le \left(1+\delta_{\max}^{D}\right)Dist_T^n \tag{29}$$

where $\delta_{\max}^{D}$ is the maximum allowable voyage distance inaccuracy; $Dist_t^n$ is the nominal voyage distance at the t-th time interval.

5. Solution Algorithm

The flow chart of the proposed method is shown in Figure 5. As illustrated in Figure 5, the PSO algorithm is used in the upper level to determine the fuel cell and battery size, and the MILP is used in the lower level to determine the optimal ship speed and hourly output of the FC and battery. PSO, developed by Kennedy and Eberhart in 1995 [36,37], is a heuristic optimization technique that is easy to implement compared with other optimization algorithms, and has been widely used in many areas [38–40]. The optimization model in the lower level is a mixed-integer nonlinear programming (MINLP) model due to the nonlinear function of Equation (2). In this paper, the piecewise linear model used in [17] is adopted to turn the nonlinear function into a linear function. Correspondingly, the MINLP model is transformed into a MILP model. MILP has many advantages over other optimization techniques, such as its ability to achieve globally optimal solutions based on the convexity of linear problems. Additionally, MILP can be solved very quickly and effectively by commercial solvers [33], especially when dealing with small-scale optimization problems. The solution algorithm is detailed as follows.

Step 1: Initialization. The initialization of PSO is implemented by randomly generating M particles with the position with N dimensions and velocity.

Step 2: Update the position and velocity of each particle. The position and velocity of each particle are updated using Equation (30).

$$\begin{cases} V_i^{k+1} = wV_i^k + c_1 r_1\left(p_{best,i}^k - X_i^k\right) + c_2 r_2\left(g_{best}^k - X_i^k\right) \\ X_i^{k+1} = X_i^k + V_i^{k+1} \end{cases} \tag{30}$$

where X_i^k and V_i^k are the position and velocity of the i-th particle in the k-th iteration, $X_i^k = \left[x_{i1}^k, x_{i2}^k, \ldots, x_{iN}^k\right]$; i is the i-th particle; k is the number of current iteration; w is the inertia weight; c_1 and c_2 are two positive constants; r_1 and r_2 are two random numbers within range [0,1]; $p_{best,i}^k$ is the previous best particle position of the i-th particle in the k-th iteration, $p_{best,i}^k = \left[x_{i1}^{p_{best}}, x_{i2}^{p_{best}}, \ldots, x_{iN}^{p_{best}}\right]$; g_{best}^k is the global best particle position in the k-th iteration, $g_{best}^k = \left[x_1^{g_{best}}, x_2^{g_{best}}, \ldots, x_N^{g_{best}}\right]$.

In order to enhance the performance of the algorithm, a dynamic update method of inertia weight is adopted, as shown in Equation (31). This approach ensures the strong global search ability of the algorithm at the beginning of the iteration with a larger inertia weight, and the accurate local search ability in later iterations with a smaller inertia weight.

$$w = w_{\max} - \frac{(w_{\max} - w_{\min})}{k_{\max}} \cdot k \tag{31}$$

where $w_{\max}$ and $w_{\min}$ are the maximum and minimum inertia weights, respectively; $k_{\max}$ is the maximum iteration number.

Step 3: Fitness calculation. Based on the given capacity of the FC and battery delivered from the upper level, the model in the lower level is optimized to minimize the operation cost of the AES. Once this optimization of the lower level is complete, the fitness of the upper level can be calculated using Equation (5) based on its corresponding fitness of the lower level.

Step 4: Update the global best particle g_{best}^{k} and current best particle $p_{best,i}^{k}$. After the fitness of all particles is calculated, the global and present best particle position is updated.

Step 5: Repeat Steps 2–5 until the stopping criterion of the algorithm is satisfied.

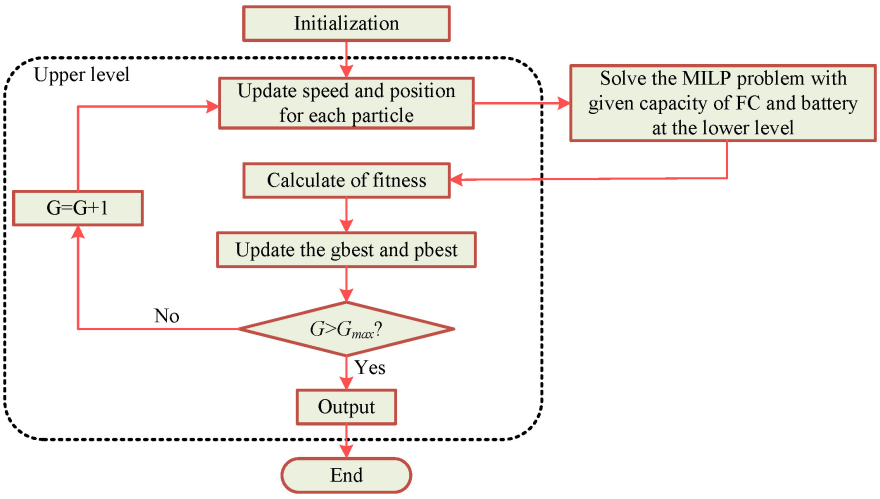

Figure 5. Flow chart of the proposed method.

6. Case Study

6.1. System Configuration

In this paper, a fuel cell/battery passenger ferry is applied in the case study. The navigation route is shown in Figure 6. The system parameters for the case study are detailed in Table 1. The service loads during the voyage are demonstrated in Figure 7. These parameters were obtained from refs. [17,18].

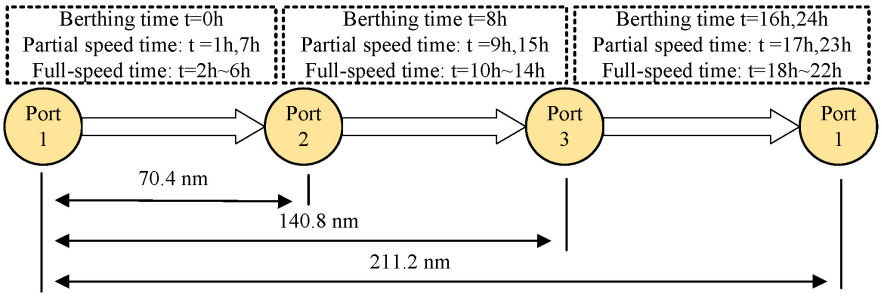

Figure 6. Navigation route for case study.

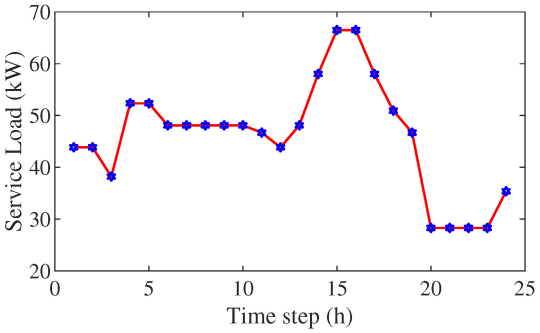

Figure 7. Service load profile.

Table 1. System parameters for case study.

Item	Parameter of Upper level
	λ_{INV}^{FC} = 40 \$/kW, $\lambda_{INV}^{bat,E}$ = 17.8 \$/kWh, $\lambda_{INV}^{bat,P}$ = 17.8 \$/kW $T_{op,lifetime}^{FC}$ = 40,000 h, $N_{lifetime}^{bat,cycle}$ = 1460 times P_{sizing}^{bat} = 300 kW, E_{sizing}^{bat} = 800 kWh, P_{sizing}^{FC} = 800 kW
Voyage	ΔT =1 h, T = 24 h v_n = 11 knots, c_1 = 0.346, c_2 = 3, η_P = 0.7, $\delta_{\max}^{v}$ = 18%, $\delta_{\max}^{D}$ = 1% T_c = {2, . . ., 6, 10, . . ., 14, 18, . . ., 22}, T_p = {1, 7, 9, 15, 17, 23}, T_b = {8, 16, 24}
Fuel cell and Hydrogen tank	$\alpha^{FC} = 1.776$, $\beta^{FC} = -41.44$, $M_{\max}^{H_2}$ = 450 kg, K^{E-m} = 0.03 kg/kWh, λ^{H_2} = 5 \$/kg $I_{\max}^{FC}$ = 0.9, $I_{\min}^{FC}$ = 0.1,$r_{\max}^{FC}$ = 50%, $r_{\min}^{FC}$ = −50%, η_R = 15%, η_{tank} = 10%
Battery	$SOC_{\max}$ = 0.9, $DoD_{\max}$ = 0.8, η_{ch} = 85%, η_{dc} = 100%, δ^{SOC} = 1%, SOC_0 = 0.5
Cold ironing	$P_{\max}^{CI}$ = 150 kW, $\lambda_t^{CI} = \begin{cases} 0.32\$/kWh & t \in \{2,\ 3,\ 4,\ 13,\ 14\} \\ 0.16\$/kWh & t \in \{1,\ 5,\ \ldots,\ 12,\ 15,\ 16\} \\ 0.07\$/kWh & t \in \{17,\ \ldots,\ 24\} \end{cases}$

6.2. Optimization Results

In this section, three cases are designed to verify the effectiveness of the proposed method, and their results are compared with each other.

Case 1: Optimal result analysis under optimal energy management but without voyage scheduling.

Case 2: Optimal result analysis by proposed method considering FC only.

Case 3: Optimal result analysis by proposed method considering FC and battery.

The results of the optimal sizing scheme, investment cost, and operation cost for each case are listed in Table 2. The ship speed at each time interval for different cases is shown in Figure 8. The results of generation scheduling and the ship electric load for Cases 1–3 are shown in Figures 9–11, respectively.

Table 2. Optimization results summary.

Item	Case 1	Case 2	Case 3
Maximum power of FC $P_{\max}^{FC}$ (kW)	591	683	501
Maximum capacity of battery $E_{\max}^{bat}$ (kWh)	243	-	243
Maximum power of battery $P_{\max}^{bat}$ (kW)	161	-	152
Investment cost of FC(\$)	23,640	27,320	20,040
Investment cost of battery (\$)	7191.2	-	7031
Total investment cost (\$)	30,831.2	27,320	27,071
Daily investment cost of FC (\$)	13.59	14.34	11.52
Daily investment cost of battery (\$)	14.78	-	14.45
Total daily investment cost (\$)	28.37	14.34	25.97
Daily consumed mass of H_2 (L)	455.01	446.11	430.90
Daily operation cost of H_2 (\$)	2275.04	2230.57	2154.50
Daily operation cost of cold ironing (\$)	58.50	20.97	58.47
Total daily operation cost (\$)	2333.54	2251.54	2212.98
Total daily cost (\$)	2361.91	2265.88	2238.95

Case 1: In this case, energy management is introduced to achieve optimal energy dispatch, and voyage scheduling is not considered, which means that the ship is assumed to sail at the nominal speed at each time interval. By observing Table 2, the planning FC capacity is 591 kW, and the planning battery capacity and power are 243 kWh and 161 kW. The investment costs for the FC and battery are \$23,640 and \$7191.2. Among the three cases, Case 1 has the highest total investment cost of \$30,831.2 and total daily cost of \$2361.91, primarily due to its high ship speed in the full-speed cruising period, as shown in Figure 8, which will require the huge installed capacity of the components and high

fuel consumption. In Figure 9, the power of the FC and the battery is utilized to meet the demands of shiploads in the full- and partial-speed cruising periods. During the berthing period, the power of the FC and cold ironing is used to meet the demands of shiploads and charge the battery.

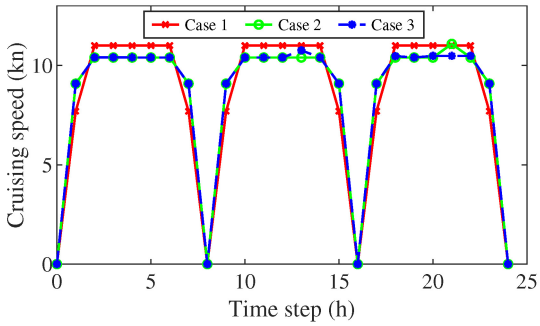

Figure 8. Ship speed at each time interval for different cases.

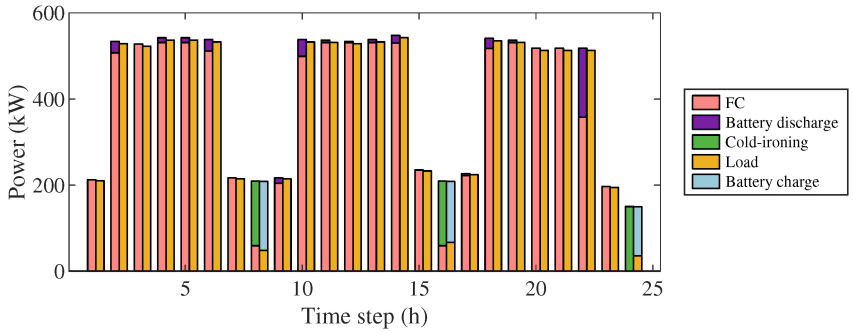

Figure 9. Generation scheduling and the ship electric load in Case 1.

Case 2: The FC is adopted as the sole energy source in this case. In Table 2, despite having the largest FC capacity of 683 kW among the three cases, Case 2 has the lowest daily investment cost of $14.34. The reason for this is that the battery's daily investment cost is zero, which makes a considerable difference. In Figure 10, the demands of shiploads during the full-speed and partial-speed cruising periods are satisfied by the power of FC. This leads to the higher consumed mass of hydrogen and daily operational cost of hydrogen compared to Case 3. Therefore, ESS integration is essential and unignorable. Since the price of cold ironing is lower than that of hydrogen, the power of cold ironing is used to meet the demands of shiploads, and the FC is turned off during the berthing period.

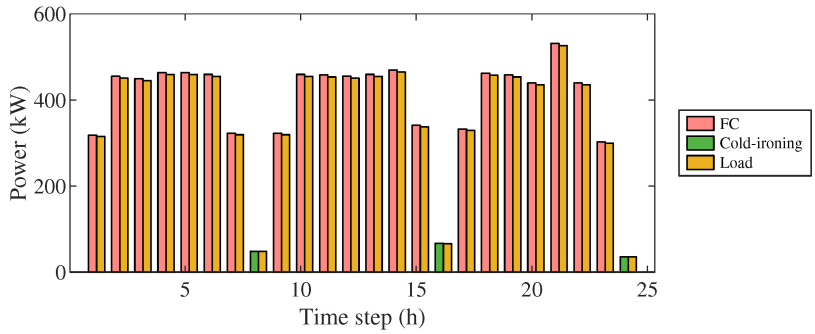

Figure 10. Generation scheduling and the ship electric load in Case 2.

Case 3: The proposed method is used in this case to investigate the impact of ESS integration and joint optimal energy management and voyage scheduling. In Table 2, Case 3 has the lowest planning FC power of 501 kW and the lowest planning battery capacity and

power of 243 kWh and 152 kW. Correspondingly, the total investment cost of Case 3 also is the lowest, with the investment cost of $20,040 for the FC and $7031 for the battery. Under optimal voyage scheduling, the ship speed is reduced in the partial-speed cruising period and increased in the full-speed cruising period, as shown in Figure 8. This led to a decrease in shiploads of Case 1 in the full-speed cruising period and an increase in the partial-speed cruising period. On this basis, the power demand in Figure 11 is decreased in the full-speed cruising period and increased in the partial-speed cruising period, resulting in decreased total fuel consumption. In Table 2, the daily consumed mass of H_2 decreases from 455.01 L to 430.90 L, a reduction of 5.3%. Then, the daily operation cost of H_2 is reduced from $2333.54 in Case 1 to $2212.98 in Case 3, while the cost of cold ironing remains similar for both cases. So, the total daily cost is reduced from $2361.91 in Case 1 to $2238.95 in Case 3, a reduction of 5.2%. In addition, although the ship speed at each time interval of Case 2 and Case 3 are similar, the ESS integration in Case 3 allows for a portion of the fuel consumption to be shared by the battery, which is charged at a lower price in the port. Thus, the daily operation cost of Case 1 is lower than that of Case 2. Ultimately, Case 3 is demonstrated to be the most economical sizing scheme, with the lowest total investment cost and total daily cost among the three cases.

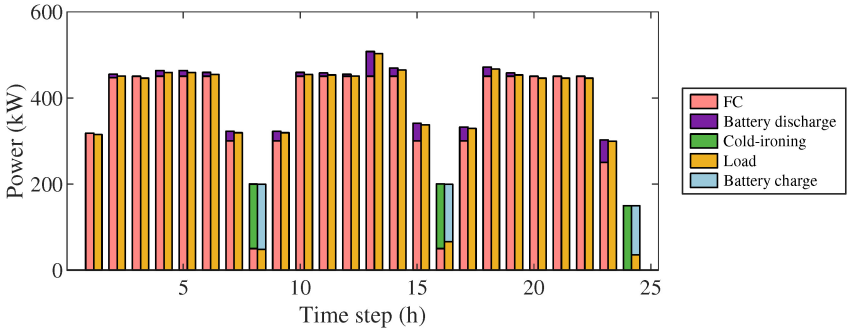

Figure 11. Generation scheduling and the ship electric load in Case 3.

The SOC profiles of the three cases are illustrated in Figure 12. In Figure 12, the battery in Cases 1 and 3 is mainly discharged in the cruising period and charged in the berthing period. However, the maximum depths of discharge (DoDs) during the voyage of Case 1 and Case 3 are 0.79 and 0.66, respectively. The smaller maximum DoD in Case 3 is more beneficial to the health of the battery. The reason behind this is that the heavier load in Case 1 requires a larger DoD to maintain a balance between the energy source and loads. Thus, the proposed optimal sizing method could help improve the performance of ESS and the overall system efficiency.

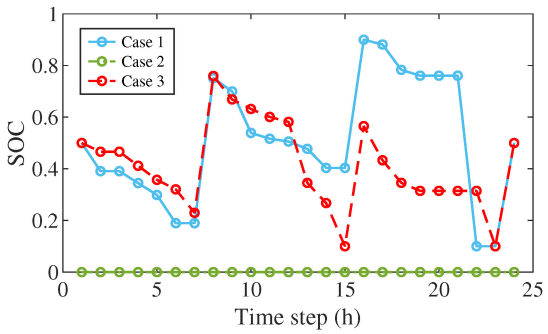

Figure 12. SOC profile for each case.

In order to illustrate the computation efficiency of the algorithm of the improved PSO used in this paper, its result is compared to that of the proposed method solved by other famous metaheuristic algorithms, such as the genetic algorithm (GA) [41], Archimedes optimization algorithm (AOA) [42], and the original PSO. These algorithms have been set

with the same population size and iteration number and tested under Intel Core i7 and GPU 3.69 GHz. The iteration figures of these algorithms are described in Figure 13. As can be seen from the figure, the improved PSO algorithm converges at a higher descending speed and has a superior optimal fitness value compared to other algorithms. Therefore, the computation efficiency of adopting the improved PSO to solve the proposed method is confirmed.

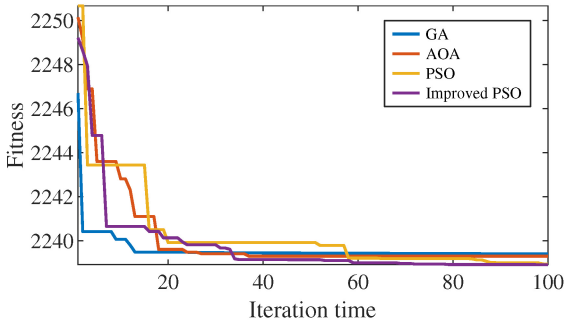

Figure 13. Iteration figure.

7. Conclusions

In this paper, the method to optimize the size of ferry components while considering joint optimal energy management and voyage scheduling is explored. First, the topology of the shipboard microgrid is analyzed, and a bilevel optimization framework is proposed to optimize the components' size and operation for the fuel cell/battery AES. Second, the mathematical model of AES voyage and hydrogen fuel cell operation is established. Third, considering the multiple operational and technical constraints, the bilevel optimal sizing and operation method is proposed. The upper level optimizes the FC and battery size by minimizing the total cost comprised of the investment and operation costs, while the lower level is used to optimize the generation and voyage scheduling of AES. Then, the PSO algorithm and MILP solver are applied to solve the upper- and lower-level optimization model, respectively. Finally, a case study is performed on a passenger ferry, demonstrating the proposed method's validity and superiority. The results show that the proposed method can reduce the total consumed mass of hydrogen by 5.3% and total daily cost by 5.2% compared with the AES using fixed voyage scheduling. The necessity of ESS integration on board is also proved in this paper.

In our future study, the MPC strategy will be introduced to improve the robustness of the model, and the environment parameters of the wave, wind, shallow water, and current will be considered in the ship voyage to improve the precision of the study. In addition, the famous simulation software entitled the Hybrid Optimization Model for Multiple Energy Resources (HOMER) will also be explored on the components sizing problem of the hybrid-powered ship.

Author Contributions: Conceptualization, H.J. and X.Y.; methodology, H.J. and X.Y.; software, H.J. and X.Y.; validation, H.J. and X.Y.; formal analysis, H.J. and X.Y.; resources, H.J.; writing—original draft preparation, H.J. and X.Y.; writing—review and editing, H.J. and X.Y.; visualization, H.J. All authors have read and agreed to the published version of the manuscript.

Funding: This research received no external funding.

Data Availability Statement: Not applicable.

Conflicts of Interest: The authors declare no conflict of interest.

References

1. Faber, J.; Hanayama, S.; Zhang, S.; Pereda, P.; Comer, B.; Hauerhof, E.; Schim van der Loeff, W.; Smith, T.; Zhang, Y.; Kosaka, H.; et al. *Fourth IMO GHG Study 2020*; Technical report; International Maritime Organization (IMO): London, UK, 2020.
2. Balcombe, P.; Brierley, J.; Lewis, C.; Skatvedt, L.; Speirs, J.; Hawkes, A.; Staffell, I. How to Decarbonise International Shipping: Options for Fuels, Technologies and Policies. *Energy Convers. Manag.* **2019**, *182*, 72–88. [CrossRef]
3. Joung, T.H.; Kang, S.G.; Lee, J.K.; Ahn, J. The IMO initial strategy for reducing Greenhouse Gas(GHG) emissions, and its follow-up actions towards 2050. *J. Int. Marit. Safety Environ. Aff. Shipp.* **2020**, *4*, 1–7. [CrossRef]
4. Gray, N.; McDonagh, S.; O'Shea, R.; Smyth, B.; Murphy, J.D. Decarbonising Ships, Planes and Trucks: An Analysis of Suitable Low-Carbon Fuels for the Maritime, Aviation and Haulage Sectors. *Adv. Appl. Energy* **2021**, *1*, 100008. [CrossRef]
5. Al-Enazi, A.; Okonkwo, E.C.; Bicer, Y.; Al-Ansari, T. A Review of Cleaner Alternative Fuels for Maritime Transportation. *Energy Rep.* **2021**, *7*, 1962–1985. [CrossRef]
6. Wan, Z.; el Makhloufi, A.; Chen, Y.; Tang, J. Decarbonizing the International Shipping Industry: Solutions and Policy Recommendations. *Mar. Pollut. Bull.* **2018**, *126*, 428–435. [CrossRef]
7. Jin, Z.; Sulligoi, G.; Cuzner, R.; Meng, L.; Vasquez, J.C.; Guerrero, J.M. Next-Generation Shipboard DC Power System: Introduction Smart Grid and dc Microgrid Technologies into Maritime Electrical Netowrks. *IEEE Electrif. Mag.* **2016**, *4*, 45–57. [CrossRef]
8. Geertsma, R.; Negenborn, R.; Visser, K.; Hopman, J. Design and Control of Hybrid Power and Propulsion Systems for Smart Ships: A Review of Developments. *Appl. Energy* **2017**, *194*, 30–54. [CrossRef]
9. Nuchturee, C.; Li, T.; Xia, H. Energy Efficiency of Integrated Electric Propulsion for Ships—A Review. *Renew. Sustain. Energy Rev.* **2020**, *134*, 110145. [CrossRef]
10. Nguyen, H.P.; Hoang, A.T.; Nizetic, S.; Nguyen, X.P.; Le, A.T.; Luong, C.N.; Chu, V.D.; Pham, V.V. The electric propulsion system as a green solution for management strategy of CO_2 emission in ocean shipping: A comprehensive review. *Int. Trans. Electr. Energy Syst.* **2021**, *31*, e12580. [CrossRef]
11. Fang, S.; Xu, Y.; Li, Z.; Zhao, T.; Wang, H. Two-Step Multi-Objective Management of Hybrid Energy Storage System in All-Electric Ship Microgrids. *IEEE Trans. Veh. Technol.* **2019**, *68*, 3361–3373. [CrossRef]
12. Xing, H.; Stuart, C.; Spence, S.; Chen, H. Fuel Cell Power Systems for Maritime Applications: Progress and Perspectives. *Sustainability* **2021**, *13*, 1213. [CrossRef]
13. Lotrič, A.; Sekavčnik, M.; Pohar, A.; Likozar, B.; Hočevar, S. Conceptual Design of an Integrated Thermally Self-Sustained Methanol Steam Reformer—High-Temperature PEM Fuel Cell Stack Manportable Power Generator. *Int. J. Hydrogren Energy* **2017**, *42*, 16700–16713. [CrossRef]
14. Pohar, A.; Hočevar, S.; Likozar, B.; Levec, J. Synthesis and Characterization of Gallium-Promoted Copper—Ceria Catalyst and Its Application for Methanol Steam Reforming in a Packed Bed Reactor. *Catal. Today* **2015**, *256*, 358–364. [CrossRef]
15. Rubin, K.; Pohar, A.; Dasireddy, V.D.; Likozar, B. Synthesis, Characterization and Activity of CuZnGaOx Catalysts for the Water–Gas Shift (WGS) Reaction for H2 Production and CO Removal after Reforming. *Fuel Process. Technol.* **2018**, *169*, 217–225. [CrossRef]
16. Shakeri, N.; Zadeh, M.; Bremnes Nielsen, J. Hydrogen Fuel Cells for Ship Electric Propulsion: Moving toward Greener Ships. *IEEE Electrif. Mag.* **2020**, *8*, 27–43. [CrossRef]
17. Banaei, M.; Rafiei, M.; Boudjadar, J.; Khooban, M.H. A Comparative Analysis of Optimal Operation Scenarios in Hybrid Emission-Free Ferry Ships. *IEEE Trans. Transp. Electrif.* **2020**, *6*, 318–333. [CrossRef]
18. Letafat, A.; Rafiei, M.; Sheikh, M.; Afshari-Igder, M.; Banaei, M.; Boudjadar, J.; Khooban, M.H. Simultaneous Energy Management and Optimal Components Sizing of a Zero-Emission Ferry Boat. *J. Energy Storage* **2020**, *28*, 101215. [CrossRef]
19. Li, Y.; Zhang, H.; Liang, X.; Huang, B. Event-Triggered-Based Distributed Cooperative Energy Management for Multienergy Systems. *IEEE Trans. Ind. Inform.* **2019**, *15*, 2008–2022. [CrossRef]
20. Shang, C.; Srinivasan, D.; Reindl, T. Economic and Environmental Generation and Voyage Scheduling of All-Electric Ships. *IEEE Trans. Power Syst.* **2016**, *31*, 4087–4096. [CrossRef]
21. Huang, Y.; Lan, H.; Hong, Y.Y.; Wen, S.; Fang, S. Joint Voyage Scheduling and Economic Dispatch for All-Electric Ships with Virtual Energy Storage Systems. *Energy* **2020**, *190*, 116268. [CrossRef]
22. Fang, S.; Gou, B.; Wang, Y.; Xu, Y.; Shang, C.; Wang, H. Optimal Hierarchical Management of Shipboard Multibattery Energy Storage System Using a Data-Driven Degradation Model. *IEEE Trans. Transp. Electrif.* **2019**, *5*, 1306–1318. [CrossRef]
23. Wen, S.; Zhao, T.; Tang, Y.; Xu, Y.; Zhu, M.; Fang, S.; Ding, Z. Coordinated Optimal Energy Management and Voyage Scheduling for All-Electric Ships Based on Predicted Shore-Side Electricity Price. *IEEE Trans. Ind. Appl.* **2021**, *57*, 139–148. [CrossRef]
24. Fang, S.; Xu, Y.; Li, Z.; Ding, Z.; Liu, L.; Wang, H. Optimal Sizing of Shipboard Carbon Capture System for Maritime Greenhouse Emission Control. *IEEE Trans. Ind. Appl.* **2019**, *55*, 5543–5553. [CrossRef]
25. Wen, S.; Zhao, T.; Tang, Y.; Xu, Y.; Zhu, M.; Huang, Y. A Joint Photovoltaic-Dependent Navigation Routing and Energy Storage System Sizing Scheme for More Efficient All-Electric Ships. *IEEE Trans. Transp. Electrif.* **2020**, *6*, 1279–1289. [CrossRef]
26. Zhao, T.; Qiu, J.; Wen, S.; Zhu, M. Efficient Onboard Energy Storage System Sizing for All-Electric Ship Microgrids via Optimized Navigation Routing under Onshore Uncertainties. *IEEE Trans. Ind. Appl.* **2022**, *58*, 1664–1674. [CrossRef]
27. Banaei, M.; Ghanami, F.; Khooban, M.H.; Boudjadar, J. Cost-effective control of Roll-on/Roll-off Emission-Free Ships. In Proceedings of the 2021 25th International Conference on Methods and Models in Automation and Robotics (MMAR), Międzyzdroje, Poland, 23–26 August 2021; IEEE: Toulouse, France, 2021; pp. 315–320.

28. Banaei, M.; Boudjadar, J.; Dragičević, T.; Khooban, M.H. Cost Effective Operation of a Hybrid Zero-Emission Ferry Ship. In Proceedings of the 2020 IEEE 11th International Symposium on Power Electronics for Distributed Generation Systems (PEDG), Dubrovnik, Croatia, 28 September–1 October 2020; IEEE: Toulouse, France, 2020; pp. 23–28.
29. Letafat, A.; Rafiei, M.; Ardeshiri, M.; Sheikh, M.; Banaei, M.; Boudjadar, J.; Khooban, M.H. An Efficient and Cost-Effective Power Scheduling in Zero-Emission Ferry Ships. *Complexity* **2020**, *2020*, 6487873. [CrossRef]
30. Han, J.; Charpentier, J.F.; Tang, T. An Energy Management System of a Fuel Cell/Battery Hybrid Boat. *Energies* **2014**, *7*, 2799–2820. [CrossRef]
31. Wang, X.; Shipurkar, U.; Haseltalab, A.; Polinder, H.; Claeys, F.; Negenborn, R.R. Sizing and Control of a Hybrid Ship Propulsion System Using Multi-Objective Double-Layer Optimization. *IEEE Access* **2021**, *9*, 72587–72601. [CrossRef]
32. Pan, X.; Zhu, X.; Zhao, F. More Environmental Sustainability Routing and Energy Management for All Electric Ships. *Front. Energy Res.* **2022**, *9*, 821236 . [CrossRef]
33. Urbanucci, L. Limits and Potentials of Mixed Integer Linear Programming Methods for Optimization of Polygeneration Energy Systems. *Energy Procedia* **2018**, *148*, 1199–1205. [CrossRef]
34. Angelo, J.S.; Krempser, E.; Barbosa, H.J. Differential evolution for bilevel programming. In Proceedings of the 2013 IEEE Congress on Evolutionary Computation, Cancun, Mexico, 20–23 June 2013; IEEE: Toulouse, France, 2013; pp. 470–477.
35. Kanellos, F.D. Optimal Power Management With GHG Emissions Limitation in All-Electric Ship Power Systems Comprising Energy Storage Systems. *IEEE Trans. Power Syst.* **2014**, *29*, 330–339. [CrossRef]
36. Kennedy, J.; Eberhart, R. Particle swarm optimization. In Proceedings of the ICNN'95—International Conference on Neural Networks, Perth, WA, Australia, 27 November–1 December 1995; IEEE: Toulouse, France, 1995; Volume 4, pp. 1942–1948.
37. Shi, Y.; Eberhart, R. A modified particle swarm optimizer. In Proceedings of the 1998 IEEE International Conference on Evolutionary Computation Proceedings, Anchorage, AK, USA, 4–9 May 1998; IEEE: Toulouse, France, 1998; pp. 69–73.
38. Yan, X.; Wang, K.; Yuan, Y.; Jiang, X.; Negenborn, R.R. Energy-Efficient Shipping: An Application of Big Data Analysis for Optimizing Engine Speed of Inland Ships Considering Multiple Environmental Factors. *Ocean. Eng.* **2018**, *169*, 457–468. [CrossRef]
39. Ahmed, E.M.; Rathinam, R.; Dayalan, S.; Fernandez, G.S.; Ali, Z.M.; Abdel Aleem, S.H.E.; Omar, A.I. A Comprehensive Analysis of Demand Response Pricing Strategies in a Smart Grid Environment Using Particle Swarm Optimization and the Strawberry Optimization Algorithm. *Mathematics* **2021**, *9*, 2338. [CrossRef]
40. Yu, H.; Gao, Y.; Wang, L.; Meng, J. A Hybrid Particle Swarm Optimization Algorithm Enhanced with Nonlinear Inertial Weight and Gaussian Mutation for Job Shop Scheduling Problems. *Mathematics* **2020**, *8*, 1355. [CrossRef]
41. Holland, J.H. *Adaptation in Natural and Artificial Systems*; University of Michigan Press: Ann Arbor, MI, USA, 1975.
42. Hashim, F.A.; Hussain, K.; Houssein, E.H.; Mabrouk, M.S.; Al-Atabany, W. Archimedes Optimization Algorithm: A New Metaheuristic Algorithm for Solving Optimization Problems. *Appl. Intell.* **2021**, *51*, 1531–1551. [CrossRef]